

# PIVM: DIFFUSION-BASED PRIOR-INTEGRATED VARIATION MODELING FOR ANATOMICALLY PRECISE ABDOMINAL CT SYNTHESIS

Dinglun He<sup>1\*</sup> Baoming Zhang<sup>2\*</sup> Xu Wang<sup>1\*</sup> Yao Hao<sup>3</sup> Deshan Yang<sup>4</sup> Ye Duan<sup>5</sup>

<sup>1</sup> Department of Electrical Engineering and Computer Science, University of Missouri, Columbia, MO, USA

<sup>2</sup> Department of Computer Science, The University of Texas at Dallas, Richardson, TX, USA

<sup>3</sup> Department of Radiation Oncology, Washington University in St. Louis, MO, USA

<sup>4</sup> Department of Radiation Oncology, Duke University, Durham, NC, USA

<sup>5</sup> School of Computing, Clemson University, Clemson, SC, USA

## ABSTRACT

Abdominal CT data are limited by high annotation costs and privacy constraints, which hinder the development of robust segmentation and diagnostic models. We present a Prior-Integrated Variation Modeling (PIVM) framework, a diffusion-based method for anatomically accurate CT image synthesis. Instead of generating full images from noise, PIVM predicts voxel-wise intensity variations relative to organ-specific intensity priors derived from segmentation labels. These priors and labels jointly guide the diffusion process, ensuring spatial alignment and realistic organ boundaries. Unlike latent-space diffusion models, our approach operates directly in image space while preserving the full Hounsfield Unit (HU) range, capturing fine anatomical textures without smoothing. Source code is available at this URL.

**Index Terms**— CT synthesis, Medical imaging, Diffusion models, Image generation.

## 1. INTRODUCTION

Abdominal computed tomography (CT) provides rich anatomical information essential for diagnosis and treatment planning [1, 11, 15]. However, developing robust deep learning models for abdominal CT remains challenging due to the scarcity of annotated datasets and the constraints of patient privacy. Manual delineation of organs is time-consuming and often inconsistent across institutions [2, 13], leading to limited data diversity and generalization. These factors have motivated a growing interest in generating anatomically accurate synthetic CT images to supplement real data and improve model robustness.

Earlier approaches relied on Generative Adversarial Networks (GANs) [4, 5, 14, 24], which enabled realistic image synthesis for data augmentation and modality translation [17,

23]. Yet, despite their visual realism, GAN-based methods often failed to preserve fine anatomical details and spatial consistency. More recently, diffusion models [3, 9, 10, 18] have emerged as a more stable alternative, producing high-fidelity and diverse images through likelihood-based training. Conditional diffusion models [6, 7, 12, 22] further improve structural control by conditioning on segmentation masks or metadata. However, most existing approaches operate in latent space or apply fixed intensity clipping, which compromises HU precision and weakens organ boundaries—limitations particularly critical for CT synthesis.

To address these issues, we propose the *Prior-Integrated Variation Modeling* (PIVM) framework, as illustrated in Fig. 1. PIVM predicts voxel-level intensity deviations relative to organ-wise priors derived from segmentation labels. Operating entirely in image space, it preserves the full HU range and maintains anatomical alignment while capturing subtle texture variations. For volumetric synthesis, we extend this formulation to a sequential slice-wise generation strategy that ensures smooth 3D continuity across slices.

Our main contributions are as follows. (1) We introduce a prior-integrated diffusion formulation for anatomically faithful CT synthesis. (2) We design a lightweight slice-wise strategy for efficient 3D volume generation. (3) We demonstrate that the synthetic data generated by PIVM improves downstream segmentation accuracy on the TotalSegmentator dataset [21].

## 2. METHOD

We next describe the components of the PIVM framework introduced in Fig. 1. Our goal is to synthesize anatomically consistent and realistic CT images through the proposed PIVM framework. Given a CT slice  $x^{(i)}$ , its segmentation map  $s^{(i)}$ , and an average-intensity prior  $I^{(i)}$  encoding organ-level mean HU values, we define a residual variation

$$v^{(i)} = x^{(i)} - I^{(i)}.$$

\*These authors contributed equally to this work.

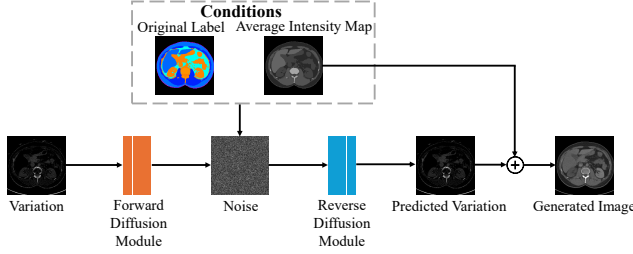


**Fig. 1.** Variation Modeling via Diffusion for CT Image Synthesis. The variation is forward diffused to Gaussian noise. A reverse diffusion model, guided by the segmentation label and average intensity map, predicts the variation signal, which is added back to reconstruct the final CT image.

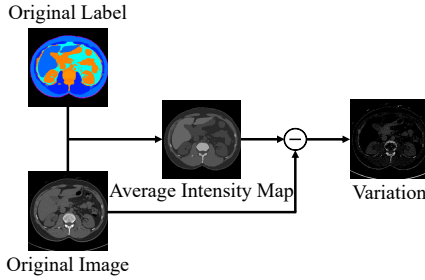


**Fig. 2.** Construction of Average Intensity Map and Variation. An average intensity map is computed from the segmentation label by replacing each organ region with its dataset-level mean value. The pixel-wise difference between the original CT image and the average map defines the variation used in subsequent diffusion modeling.

An illustration of this construction is shown in Fig. 2, where the residual variation highlights organ-level deviations from the average intensity prior. Instead of generating absolute intensities, PIVM performs diffusion on this variation, focusing learning capacity on fine structural deviations that distinguish individual anatomy from its organ-level prior.

### 2.1. Prior-Integrated Variation Modeling

Denosing Diffusion Probabilistic Models (DDPMs) [9] synthesize data by progressively denoising Gaussian noise through a learned reverse process. In PIVM, diffusion is applied to the variation map  $v^{(i)}$  rather than the full image. During training, Gaussian noise is incrementally added over  $T$  steps, and the denoising network predicts the clean variation conditioned on both the segmentation label and intensity prior:

$$\epsilon_{\theta}(v_t^{(i)}, t, s^{(i)}, I^{(i)}).$$

After denoising, the final reconstruction is obtained as

$$\hat{x}_0^{(i)} = I^{(i)} + \hat{v}_0^{(i)}.$$

This formulation teaches the model to recover localized intensity deviations from anatomical averages, improving boundary precision and HU fidelity while remaining computationally efficient. A U-Net backbone serves as the denoising network, capturing both global context and fine-grained details via skip connections.

### 2.2. Sequential Slice-Wise Volume Generation

To generate full 3D volumes, PIVM is extended to a slice-wise synthesis strategy that maintains coherence across slices without the cost of full 3D diffusion. The first slice  $\hat{x}^{(1)}$  is generated from noise conditioned on its label  $s^{(1)}$  and prior  $I^{(1)}$ . Each subsequent slice  $\hat{x}^{(t)}$  is produced using the previous slice as an additional conditioning input:

$$\hat{x}^{(t)} = f_{\theta}(\hat{x}^{(t-1)}, s^{(t)}, I^{(t)}, \epsilon_t),$$

where  $\epsilon_t \sim \mathcal{N}(0, I)$  represents Gaussian noise scaled to local intensity statistics. Conditioning on the prior slice encourages smooth transitions and consistent boundaries throughout the 3D volume, implicitly enforcing long-range anatomical continuity. This design achieves a strong balance between realism and efficiency, providing high structural fidelity at a fraction of the memory cost of volumetric diffusion models.

## 3. EXPERIMENTS AND RESULTS

### 3.1. Dataset and Preparation

We trained and evaluated PIVM using the *TotalSegmentator* dataset [21], which comprises 1,228 clinical CT volumes annotated for 117 anatomical structures. For this study, 865 abdominal scans were selected, each containing between 100 and 600 axial slices. To balance anatomical coverage and computational load, we extracted 12,853 representative 2D slices and standardized all images to  $256 \times 256$  pixels through resampling and zero-padding. Each slice was paired with segmentation masks for 34 major organs, including the liver, spleen, kidneys, and pancreas.

All intensities were converted to HU using DICOM metadata and clipped to  $[-200, 300]$  solely for the construction of *average-organ-intensity maps*. These maps encode coarse structural priors that guide the diffusion process. The original intensity range was later restored after residual prediction.

For each organ  $k$ , we computed a global mean intensity  $\mu_k$  across the training data:

$$\mu_k = \frac{\sum_i \sum_{(u,v) \in \Omega_k^{(i)}} x_{u,v}^{(i)}}{\sum_i |\Omega_k^{(i)}|}, \quad \text{where } \Omega_k^{(i)} = \{(u, v) : s_{u,v}^{(i)} = k\}.$$

Each slice-specific prior map  $I^{(i)}$  was then constructed as:

$$I_{u,v}^{(i)} = \begin{cases} \mu_k, & \text{if } s_{u,v}^{(i)} = k, \\ 0, & \text{otherwise.} \end{cases}$$

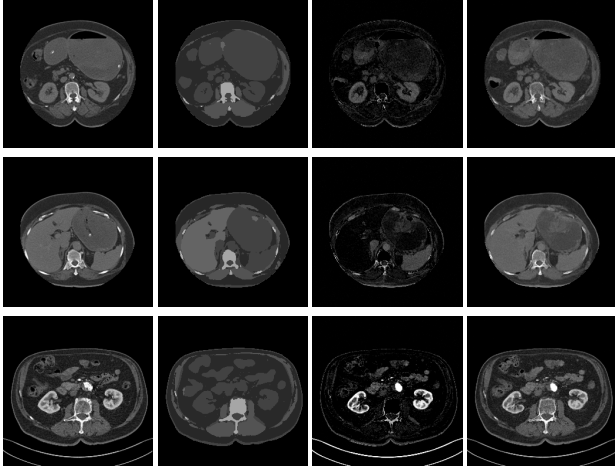


**Fig. 3.** Examples of PIVM’s generation process. Columns show the ground-truth CT image, the corresponding average organ intensity priors, the predicted intensity variations, and the reconstructed CT obtained by combining the prior with the variation.

These priors preserve anatomical layout while providing an intensity baseline for the variation-prediction stage.

### 3.2. Implementation Details

The diffusion backbone adopted a U-Net architecture for the denoising network  $\epsilon_\theta(x_t, t)$ , equipped with symmetric skip connections to capture both global context and fine anatomical detail. Training was performed on 12,853 abdominal CT slices using the Adam optimiser ( $\beta_1 = 0.9, \beta_2 = 0.99$ ) with an initial learning rate of  $1 \times 10^{-4}$ , halved every 20 epochs. Each batch contained 32 slices, and convergence was typically reached by around the 200<sup>th</sup> epoch. All experiments were executed on a single NVIDIA RTX 4090 GPU, and end-to-end training of the complete framework required approximately 36 hours.

For qualitative comparison, we reproduced the MAISI framework [7] using its official MONAI implementation. All architectural and training configurations followed the released model without modification, except for dataset paths and output settings. MAISI was executed in segmentation-to-image mode with its default preprocessing, which applies fixed HU clipping to the range  $[-1000, 1000]$ .

To assess image fidelity, we employed the Structural Similarity Index Measure (SSIM) [20] and the Fréchet Inception Distance (FID) [8]. For 3D volumes, visual inspection by experienced radiologists was used to evaluate spatial continuity and anatomical plausibility.

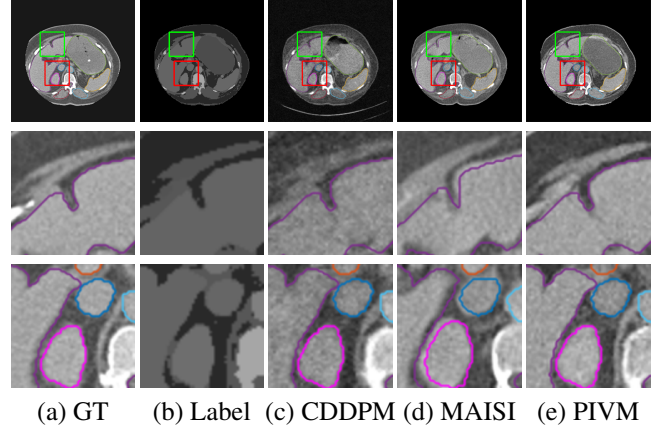


**Fig. 4.** Zoomed-in comparison of synthesis quality. Columns display: (a) ground-truth CT, (b) segmentation labels, (c) CD-DPM outputs, (d) MAISI outputs, and (e) PIVM outputs.

### 3.3. Results

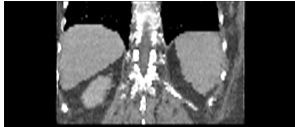
**Quantitative Results.** We use CDDPM [19] as our full-image diffusion baseline. The model operates directly in the image domain and predicts absolute HU values from noisy inputs using only the segmentation mask, without any organ-wise intensity priors. Notably, CDDPM can be regarded as PIVM without the variation modeling step, since diffusion is applied directly to the full CT image. This setup provides a clear reference point for assessing the contribution of variation-based modeling in PIVM. Representative qualitative results of PIVM are shown in Fig. 3. The synthesized CT images exhibit strong spatial alignment with the segmentation masks and preserve fine anatomical details. As illustrated in Fig. 4, MAISI and CDDPM tend to generate over-smoothed textures due to latent-space sampling and HU clipping, while PIVM maintains subtle structural variations by operating directly in image space and preserving the full HU range.

**Qualitative Results.** Quantitative results are summarized in Table 1. PIVM achieves the best average reconstruction performance across five representative patients, with higher mean SSIM and lower mean FID than CDDPM and MAISI.

**3D Volume Visualization.** To evaluate volumetric coherence, we extended PIVM to sequentially synthesize 3D abdominal CT volumes slice by slice, as described in Section 2. Representative coronal and sagittal views of a generated volume are shown in Fig. 5. The model preserves smooth inter-slice continuity and reconstructs major abdominal structures with realistic morphology, demonstrating that it effectively captures long-range spatial relationships. Expert inspection confirmed that the synthesized volumes exhibit anatomically plausible organ shapes and boundary transitions suitable for visualization, education, and training scenarios.

**Table 1.** Comparison of SSIM and FID among CDDPM, MAISI, and PIVM.

Patient	SSIM $\uparrow$			FID $\downarrow$		
	CDDPM	MAISI	PIVM (ours)	CDDPM	MAISI	PIVM (ours)
1	0.231	0.742	<b>0.846</b>	117.66	133.70	<b>63.12</b>
2	0.254	0.755	<b>0.817</b>	98.12	<b>69.91</b>	75.59
3	0.364	0.638	<b>0.716</b>	<b>70.09</b>	117.91	72.71
4	0.248	0.702	<b>0.825</b>	117.53	145.44	<b>71.54</b>
5	0.280	0.705	<b>0.799</b>	91.61	121.49	<b>54.12</b>
Avg. $\pm$ sd	0.275 $\pm$ 0.053	0.708 $\pm$ 0.046	<b>0.801<math>\pm</math>0.050</b>	99.00 $\pm$ 19.89	117.69 $\pm$ 28.83	<b>67.42<math>\pm</math>8.76</b>



(a) Coronal view



(b) Sagittal view

**Fig. 5.** Multi-view visualization of a generated 3D abdominal CT volume, illustrating anatomical fidelity and inter-slice continuity. Left: coronal view with overlaid multi-organ contours. Right: sagittal view of the same volume.**Table 2.** Segmentation Performance Comparison for Models Trained on Datasets Generated by CDDPM, MAISI, and PIVM.

Metric	CDDPM	MAISI	PIVM (ours)
Hausdorff Distance ( $\downarrow$ )	52.95	61.21	<b>43.16</b>
Average Surface Dist. ( $\downarrow$ )	13.23	17.36	<b>6.60</b>
mIoU ( $\uparrow$ )	0.30	0.27	<b>0.48</b>
Dice Coefficient ( $\uparrow$ )	0.38	0.34	<b>0.53</b>

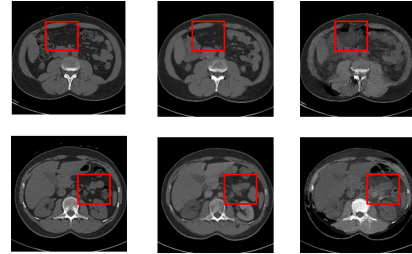
### 3.4. Downstream Segmentation Task

In Table 2, we evaluate the use of PIVM-generated images in a downstream segmentation task. A U-Net model [16] was trained on 5,000 synthetic slices produced by each method. Models trained with PIVM data consistently outperform those trained on CDDPM and MAISI across all metrics. This reflects improved boundary accuracy and region-level overlap.

We further examined the utility of PIVM-generated data in a downstream segmentation task with same segmentation configurations: (1) a real dataset of 5,000 annotated slices, (2) 5,000 synthetic slices generated by PIVM, and (3) a hybrid dataset combining both sources. As summarized in Table 3, the hybrid dataset yields the strongest overall performance. This demonstrates that PIVM-generated data provide effective augmentation for downstream segmentation.

### 3.5. Ablation Study

To investigate the impact of segmentation label granularity on image synthesis quality, we varied the number of conditioning classes, as illustrated in Fig. 6. Using only 13 labels

**Fig. 6.** Image generation results under different conditions. From left to right: ground truths (GT), images generated from 34 labels, and images generated from 13 labels.

produced partially coherent structures but led to noticeable loss of fine details, particularly around skeletal regions. In contrast, incorporating all 34 labels resulted in more realistic images with clearer anatomical boundaries and complete organ delineation.

**Table 3.** Segmentation Performance for Models Trained on Original Dataset, Generated Dataset, and Combined Dataset.

Metric	Original Dataset	Generated Dataset	Combined Dataset
Hausdorff Distance ( $\downarrow$ )	23.54	43.16	<b>22.24</b>
mIoU ( $\uparrow$ )	0.78	0.48	<b>0.81</b>
Dice Coefficient ( $\uparrow$ )	0.87	0.53	<b>0.88</b>

## 4. CONCLUSION

This work presents PIVM, a diffusion-based approach to synthesising anatomically precise abdominal CT images. By modeling voxel-wise deviations from organ-specific intensity priors, the method retains the entire HU range and preserves the fine structural detail that is often blurred by conventional latent-space diffusion. Both visual assessment and quantitative evaluation show that PIVM produces smoother organ boundaries and more realistic tissue contrasts, supporting its potential for data augmentation and simulation in medical imaging. However, some residual artefacts, particularly in

small vessels and diaphragmatic regions, reflect the limitations of current label resolution and sampling balance. Future improvements may come from finer-grained conditioning and fully volumetric generation. Overall, PIVM shows that incorporating explicit anatomical information into diffusion modeling can produce synthetic CT data that are both realistic and clinically interpretable.

## 5. COMPLIANCE WITH ETHICAL STANDARDS

This study was conducted using fully anonymised, publicly available human CT data from open-access sources. According to the data usage licence, formal ethical approval was not required.

## 6. ACKNOWLEDGMENTS

This research was supported by the National Institute of Biomedical Imaging and Bioengineering (NIBIB) under grant R01-EB029431, with partial support from the Department of Radiation Oncology, Washington University School of Medicine in St. Louis.

## 7. REFERENCES

- [1] F De Muzio, C Cutolo, V Granata, R Fusco, L Ravo, N Maggiale, MC Brunese, R Grassi, F Grassi, F Bruno, et al. Ct study protocol optimization in acute non-traumatic abdominal settings. *Eur. Rev. Med. Pharmacol. Sci*, 26:860–878, 2022.
- [2] A Omar Adil Deheyab, Mohammed Hasan Alwan, Islam khalid Abdul Rezzaq, Omar Abdulkareem Mahmood, Yousif I Hammadi, Ali Noori Kareem, and Maha Ibrahim. An overview of challenges in medical image processing. In *Proceedings of the 6th International Conference on Future Networks & Distributed Systems*, pages 511–516, 2022.
- [3] Prafulla Dhariwal and Alex Nichol. Diffusion models beat gans on image synthesis, 2021.
- [4] Ian Goodfellow, Jean Pouget-Abadie, Mehdi Mirza, Bing Xu, David Warde-Farley, Sherjil Ozair, Aaron Courville, and Yoshua Bengio. Generative adversarial nets. *Advances in neural information processing systems*, 27, 2014.
- [5] Ishaan Gulrajani, Faruk Ahmed, Martin Arjovsky, Vincent Dumoulin, and Aaron C Courville. Improved training of wasserstein gans. *Advances in neural information processing systems*, 30, 2017.
- [6] Alper Gungör, Salman UH Dar, Şaban Öztürk, Yılmaz Korkmaz, Hasan A Bedel, Gokberk Elmas, Muzaffer Ozbey, and Tolga Çukur. Adaptive diffusion priors for accelerated mri reconstruction. *Medical Image Analysis*, 88:102872, 2023.
- [7] Pengfei Guo, Can Zhao, Dong Yang, Ziyue Xu, Vishwesh Nath, Yucheng Tang, Benjamin Simon, Mason Belue, Stephanie Harmon, Baris Turkbey, et al. Maisi: Medical ai for synthetic imaging. In *2025 IEEE/CVF Winter Conference on Applications of Computer Vision (WACV)*, pages 4430–4441. IEEE, 2025.
- [8] Martin Heusel, Hubert Ramsauer, Thomas Unterthiner, Bernhard Nessler, and Sepp Hochreiter. Gans trained by a two time-scale update rule converge to a local nash equilibrium. *Advances in neural information processing systems*, 30, 2017.
- [9] Jonathan Ho, Ajay Jain, and Pieter Abbeel. Denoising diffusion probabilistic models. *Advances in neural information processing systems*, 33:6840–6851, 2020.
- [10] Amirhossein Kazerouni, Ehsan Khodapanah Aghdam, Moein Heidari, Reza Azad, Mohsen Fayyaz, Ilker Hacihaliloglu, and Dorit Merhof. Diffusion models in medical imaging: A comprehensive survey. *Medical Image Analysis*, page 102846, 2023.
- [11] Geert Litjens, Thijs Kooi, Babak Ehteshami Bejnordi, Arnaud Arindra Adiyoso Setio, Francesco Ciompi, Mohsen Ghafoorian, Jeroen Awm Van Der Laak, Bram Van Ginneken, and Clara I Sánchez. A survey on deep learning in medical image analysis. *Medical image analysis*, 42:60–88, 2017.
- [12] Qing Lyu and Ge Wang. Conversion between ct and mri images using diffusion and score-matching models. *arXiv preprint arXiv:2209.12104*, 2022.
- [13] Jun Ma, Yao Zhang, Song Gu, Cheng Zhu, Cheng Ge, Yichi Zhang, Xingle An, Congcong Wang, Qiyuan Wang, Xin Liu, et al. Abdoment-1k: Is abdominal organ segmentation a solved problem? *IEEE Transactions on Pattern Analysis and Machine Intelligence*, 44(10):6695–6714, 2021.
- [14] Xudong Mao, Qing Li, Haoran Xie, Raymond YK Lau, Zhen Wang, and Stephen Paul Smolley. Least squares generative adversarial networks. In *Proceedings of the IEEE international conference on computer vision*, pages 2794–2802, 2017.
- [15] Hyungjin Rhee and Mi-Suk Park. The role of imaging in current treatment strategies for pancreatic adenocarcinoma. *Korean Journal of Radiology*, 22(1):23, 2021.
- [16] Olaf Ronneberger, Philipp Fischer, and Thomas Brox. U-net: Convolutional networks for biomedical image segmentation. In *Medical image computing and computer-assisted intervention—MICCAI 2015: 18th international conference, Munich, Germany, October 5-9, 2015, proceedings, part III 18*, pages 234–241. Springer, 2015.
- [17] Hoo-Chang Shin, Neil A Tenenholtz, Jameson K Rogers, Christopher G Schwarz, Matthew L Senjem, Jeffrey L Gunter, Katherine P Andriole, and Mark Michalski. Medical image synthesis for data augmentation and anonymization using generative adversarial networks. In *Simulation and Synthesis in Medical Imaging: Third International Workshop, SASHIMI 2018, Held in Conjunction with MICCAI 2018, Granada, Spain, September 16, 2018, Proceedings 3*, pages 1–11. Springer, 2018.
- [18] Jiaming Song, Chenlin Meng, and Stefano Ermon. Denoising diffusion implicit models. *arXiv preprint arXiv:2010.02502*, 2020.
- [19] Xu Wang, Dinglun He, Baoming Zhang, Yao Hao, Deshan Yang, and Ye Duan. Conditional diffusion model for abdominal ct image synthesis. In *2025 IEEE 22nd International Symposium on Biomedical Imaging (ISBI)*, pages 1–5. IEEE, 2025.
- [20] Zhou Wang, Alan C Bovik, Hamid R Sheikh, and Eero P Simoncelli. Image quality assessment: from error visibility to structural similarity. *IEEE transactions on image processing*, 13(4):600–612, 2004.

- [21] Jakob Wasserthal, Hanns-Christian Breit, Manfred T Meyer, Maurice Pradella, Daniel Hinck, Alexander W Sauter, Tobias Heye, Daniel T Boll, Joshy Cyriac, Shan Yang, et al. Totalsegmentator: robust segmentation of 104 anatomic structures in ct images. *Radiology: Artificial Intelligence*, 5(5), 2023.
- [22] Yutong Xie and Quanzheng Li. Measurement-conditioned denoising diffusion probabilistic model for under-sampled medical image reconstruction. In *International Conference on Medical Image Computing and Computer-Assisted Intervention*, pages 655–664. Springer, 2022.
- [23] Xi Yang et al. Mri to ct synthesis using deep convolutional networks. *Proceedings of the International Conference on Medical Image Computing and Computer-Assisted Intervention (MICCAI)*, pages 169–177, 2018.
- [24] Jun-Yan Zhu, Taesung Park, Phillip Isola, and Alexei A Efros. Unpaired image-to-image translation using cycle-consistent adversarial networks. *Proceedings of the IEEE international conference on computer vision*, pages 2223–2232, 2017.